Autocatalytic DNAzyme Assembly for Amplified Intracellular Imaging

*Keke Gong,† Qiong Wu,† Hong Wang, Shizhen He, Jinhua Shang and Fuan Wang**

College of Chemistry and Molecular Sciences, Wuhan University,

Wuhan, Hubei, 430072, P. R. China

* To whom correspondence should be addressed. E-mail: fuanwang@whu.edu.cn

† These authors contributed equally to the paper as first authors.

Table of Contents

Experimental Section

Materials and Instruments

4-(2-Hydroxyethyl) piperazine-1-ethanesulfonic acid sodium salt (HEPES), sodium chloride (NaCl) and magnesium chloride ($MgCl_2$) were all of analytical grade and obtained from Sigma-Aldrich without further purification. DNA marker, GelRed, fetal bovine serum (FBS) and Lipofectamine 3000 transfection Reagent were purchased from Invitrogen (Carlsbad, CA). Dulbecco's Modified Eagle Medium (DMEM) was provided by HyClone (Logan, Utah, USA). Trypsin was attained from Genview (USA). All oligonucleotides were synthesized and HPLC-purified by Sangon Biotech. Co., Ltd. (Shanghai, China). Detailed sequences were presented in **Table S1**. The ribonucleotide (rA)-containing substrate modified with fluorophore/quencher pair was bought from Takara Bio Inc. (Dalian, China). Water was purified using a Millipore Milli-Q water purification system throughout all experiments. MCF-7, HeLa and MRC-5 cells were supplied by Shanghai Institutes for Biological Sciences (SIBS). AFM images were obtained in tapping mode by Multimode 8 Atomic Force Microscope with a NanoScope V controller (Bruker). Atomic force microscope (AFM) cantilever (SCANASYST-AIR) was bought from Bruker (Camarilla, CA). Fluorescence spectra were obtained by Cary Eclipse Fluorescence Spectrophotometer (Agilent Technologies). Leica TCS-SP8 was selected for confocal microscopic imaging. The flow cytometry was performed using a CytoFLEX system (Beckman Coulter, USA) under 488 nm excitation.

Fluorescence assay

All assays were performed in HEPES buffer (10 mM, pH 7.2, 1 M NaCl, 100 mM $MgCl_2$). Here each functional DNA hairpin was heated at 95 °C for 5 min and instantly cooled down to 25 °C for at least 2 hours before use. The concentrations of $\mathbf{H_1}$, $\mathbf{H_2}$, $\mathbf{H_3}$ and $\mathbf{H_4}$ were 400 nM each to detect target **T**. And the concentrations of $\mathbf{S_{D1}}$ and **L** were 100 nM and 125 nM, respectively. For amplified detection of miRNA, the concentration of "helper" hairpin $\mathbf{H_5}$ was 100 nM while the concentrations of other probes remained at 400 nM each. Unless specified, the fluorescence spectra were acquired at 5 h.

Gel electrophoresis analysis

For gel electrophoresis assay, the concentrations of **T**, $\mathbf{H_3}$ and $\mathbf{H_4}$ were 300 nM each, the concentrations of $\mathbf{H_1}$ and $\mathbf{H_2}$ were 600 nM each, and the concentrations of $\mathbf{S_{D1}}$ and **L** were 100

nM and 125 nM, respectively. All reactants were incubated in HEPES buffer (10 mM, pH 7.2, 1 M NaCl, 100 mM $MgCl_2$) for 5 h at 25 °C. Then, 2 μL 6× loading buffer was added into each sample (10 μL) and the mixture was loaded into the notches of a freshly prepared 9% native polyacrylamide gel. Electrophoresis was conducted at a fixed voltage of 100 V in 1×TBE buffer (89 mM Tris, 89 mM boric acid, 2.0 mM EDTA, pH 8.3) for 4 h. Then the gel was stained with GelRed and viewed by FluorChem FC3 (ProteinSimple, USA) under UV irradiation (λ=365 nm).

Atomic force microscopy (AFM) imaging

In order to obtain the AFM image of F-HCR-DNAzyme-generated linear copolymeric duplex nanowires, the reaction was conducted in HEPES buffer (10 mM, pH=7.2, 1 M NaCl, 100 mM $MgCl_2$) that containing $\mathbf{H_1}$ + $\mathbf{H_2}$ + $\mathbf{H_3}$ + $\mathbf{H_4}$ (200 nM each) and trigger **T** (25 nM). The freshly cleaved mica surface was modified with $MgCl_2$ (2 mM) for 2 min to obtain positive charges on its surface for the adsorption of DNA samples. Then the mica was rinsed with ultrapure water and then was dried in nitrogen atmosphere. The resultant F-HCR-DNAzyme dsDNA product was diluted with ultrapure water, and then was deposited on the mica surface for 15 min to ensure an efficient adhesion.

Colorimetric assay

All samples were prepared in HEPES buffer (10 mM, pH=7.2, 1 M NaCl and 100 mM $MgCl_2$). Firstly, the $\mathbf{S_{D1}}$ (100 nM), **L** (125 nM), $\mathbf{H_1}$ (400 nM), $\mathbf{H_6}$ (400 nM), $\mathbf{H_3}$ (400 nM), $\mathbf{H_7}$ (400 nM) and auxiliary hairpin $\mathbf{H_5}$ (100 nM) were reacted with miR-21 in HEPES buffer for 5 h. Then, 22 μL hemin (100 μM) was added to the reaction mixture and incubated for another 30 min to form hemin/G-quadruplex DNAzyme (110 μL). Finally, 22 μL $ABTS^{2-}$ (10 mM), 22 μL H_2O_2 (5 mM), and 66 μL buffer were added and incubated for 5 min to immediately acquire their ultraviolet absorption spectra.

Cell imaging

MCF-7 and HeLa cells were incubated in Dulbecco's Modified Eagle Medium (DMEM) with 10% FBS and 1% penicillin/streptomycin at 37 °C in a humid atmosphere of 5% CO_2. MRC-5 cells were incubated in Minimum Essential Medium (MEM) with 10% FBS and 1% penicillin/streptomycin at 37 °C in a humid atmosphere of 5% CO_2. Cells were incubated in 20 mm confocal plate for 12 h before transfection. The F-HCR-DNAzyme mixture containing

H_5 (0.1 μM), **H_1** (0.2 μM), **H_2** (0.2 μM), **H_3** (0.2 μM), **H_4** (0.2 μM), **S_{D1}** (0.2 μM), **L** (0.25 μM) and **S_{D2}** (0.2 μM) was added into Opti-MEM (200 μL), and then was mixed with lipofectamine 3000 (5 μL) diluted in Opti-MEM (200 μL) for 10 min. Then these cells were transfected with 75 μL FBS at 37 °C for 4 h prior to PBS washing for fluorescence imaging. For the Non-F-HCR-DNAzyme imaging experiment, the substrate **S_{D1}** (0.2 μM) was replaced with **S_{D1}'** (0.2 μM), and other components remained the same. For the anti-miRNA inhibitor experiment, MCF-7 cells were cultured with anti-miR-21 inhibitor oligonucleotide (final concentration, 100 nM) for 1 h, followed by further transfection and incubation with the F-HCR-DNAzyme system for 4 h. An external excitation of 488 nm was selected for the green channel of FAM. All images were performed at 63× objective lens with water. The fluorescence intensity of the acquired confocal images was firstly calculated with ImageJ software, and then the scatter diagrams of obtained fluorescence intensity at each selected confocal image was collected by using the GraphPad Prism 5.0 software.

Flow cytometric analysis

MCF-7, HeLa and MRC-5 cells were seeded in a twelve-well culture plate and cultured at 37 °C for 12 h. Then the MCF-7 cells were transfected with the F-HCR-DNAzyme system (0.2 μM **H_1**, **H_2**, **H_3**, **H_4**, **S_{D1}**, **S_{D2}**, 0.1 μM **H_5** and 0.25 μM **L**) or the Non-F-HCR-DNAzyme system (0.2 μM **H_1**, **H_2**, **H_3**, **H_4**, **S_{D1}'**, **S_{D2}**, 0.1 μM **H_5** and 0.25 μM **L**). For the inhibitor experiment, the MCF-7 cells were treated with anti-miR-21 inhibitor oligonucleotide (final concentration, 100 nM) for 1 h prior to the F-HCR-DNAzyme components (0.2 μM **H_1**, **H_2**, **H_3**, **H_4**, **S_{D1}**, **S_{D2}**, 0.1 μM **H_5** and 0.25 μM **L**). The HeLa and MRC-5 cells were transfected with the F-HCR-DNAzyme system (0.2 μM **H_1**, **H_2**, **H_3**, **H_4**, **S_{D1}**, **S_{D2}**, 0.1 μM **H_5** and 0.25 μM **L**). After 4 h transfection, cells were washed with 1× PBS for three times and digested from the twelve-well culture plate by trypsin. Then these cells were centrifuged at 1200 rpm for 3 min and re-dispersed in 500 μL 1× PBS. Fluorescence intensities represented 10^4 analyzed cells.

Table S1. The DNA sequences used in this work.

No.	Sequence (5'→3')
H_1	5'-TAC ACT GAG AGA TGA AGA TGA AGC CAT ACC GCT TCA TCT TCA TCT CTC TAG GCA CCC ATG TTA CAC T-3'
H_2	5'-TCA TTC AGC GAT CCAA GCT TCA TCT TCA TCT CTC GTT TTG GAG AGA TGA AGA TGA AGC GGT ATG-3'
H_3	5'-CTG CTC AGC GAT CCT ACA AAA CGA GAG ATG AAG ATG AAG CAA CCA GGC TTC ATC TTC ATC TCT C-3'
H_4	5'-GCT TCA TCT TCA TCT CTC AGT GTA GAG AGA TGA AGA TGA AGC CTG GTT TTG GCA CCC ATG TAC AGT C-3'
H_5	5'-ATC AGA CTG ATG TTG ATA GCT TCA TCT TCA TCT CTC AGT GTA TCA ACA TCA GTC TGA TAA GCT A-3'
H_6	5'-CCG CCG CTT CAT CTT CAT CTC TCG TTT TGG AGA GAT GAA GAT GAA GCG GTA TGT GGG TAG GGC GGG TTG GG-3'
H_7	5'-GCT TCA TCT TCA TCT CTC AGT GTA GAG AGA TGA AGA TGA AGC CTG GTT -3'
H_{5A}	5'-ATC AGA CTG ATG TTG ATAC GCT TCA TCT TCA TCT CTC AGT GTA TCA ACA TCA GTC TGA TAA GCT A-3'
H_{5B}	5'-ATC AGA CTG ATG TTG A GCT TCA TCT TCA TCT CTC AGT GTA TCA ACA TCA GTC TGA TAA GCT A-3'
S_{D2}	5'-TGA CTG TTrA GGA ATG AC-3'
S_{D1}	5'-GCT TCA TCT TCA TCT CTC AGT GTA TrAG GAG CAG TTA GGC TAT TCG GCA CAA GTG G-3'
$S_{D1'}$	5'-GCT TCA TCT TCA TCT CTC AGT GTA TAG GAG CAG TTA GGC TAT TCG GCA CAA GTG G-3'
L_{15}	5'-CCA CTT GTG CCG AAT AGC CTA AAA GAT AAG ATG TAG ATC AAG C-3'
L_{14}	5'-CCA CTT GTG CCG AAT AGC CTA AAA GAT AAG ATG AAG-3'
L_{16}	5'-CCA CTT GTG CCG AAT AGC CTA AAA GAT AAG ATC TAG ATC AAG C-3'
T	5'-GCT TCA TCT TCA TCT CTC AGT GTA-3'
T_A	5'-GCT TCA TCT TCA TC**A** CTC AGT GTA-3'
T_B	5'-GCT TCA TCT TCA TCA CTC AG**A** GTA-3'
T_C	5'-GCT TCA **A**CT TCA TCA CTC AG**A** GTA-3'
miR-21	5'-UAG CUU AUC AGA CUG AUG UUG A-3'
miR-155	5'-UUA AUG CUA AUC GUG AUA GGG GU-3'
miR-199a	5'-GUC ACA GUA GUC UGC ACA U-3'
let-7a	5'-UGA GGU AGU AGG UUG UAU AGU U-3'
anti-miR-21	5'-UCA ACA UCA GUC UGA UAA GCU A-3'

Table S2. Comparison of different microRNA detection strategies.

Systems	Sensing Duration (h)	LOD (M)	Ref.
Cascaded HCR-DNAzyme system for amplified detection of miRNA	12	1.0×10^{-14}	[1]
HCR for cancer-related miRNA detection of live cells	4	1.8×10^{-11}	[2]
Feedback CHA-DNAzyme system for detecting miRNA	5	1.3×10^{-11}	[3]
DNAzyme-based nanomachine for miRNA detection in living cells	6	1.0×10^{-10}	[4]
Non-feedback HCR-DNAzyme system for nucleic acid detection	5	1.0×10^{-9}	This work
Feedback HCR-DNAzyme system for nucleic acid detection	5	1.0×10^{-11}	This work

Schematic illustration of the F-HCR-DNAzyme system

As shown in **Figure S1**, the isothermal autonomous cross-activated HCR-DNAzyme system starts with the HCR procedure that consisting of four functional hairpins **H_1**, **H_2**, **H_3** and **H_4**. **H_1** contains the domain a-b (red) that is complementary to trigger (**T**) while the sequence b-c* (green) of **H_2** is complementary to the domain c-b* (red) of **H_1**. The domain b-e* (red) of **H_3** can further recognize and hybridize with the sequence e-b*(green) of **H_2** while the sequence b-g* (green) of **H_4** is complementary to domain g-b* (red) of **H_3**. Each of these hairpins is furtherly elongated with a DNAzyme subunit (from the split E6-type Mg^{2+}-dependent DNAzyme), resulting in an inactive DNAzyme structure. These hairpins coexist without cross-hybridization due to the formation of a stable hairpin structure. The analyte **T** opens **H_1** *via* the toehold-mediated strand displacement, resulting in the formation of hybrid **T-H_1**. The generated single-stranded domain c-b* (red) then unfolds **H_2** to assemble an intermediate structure **T-H_1·H_2**. The newly exposed sequence e-b* opens hairpin **H_3** to form **T-H_1·H_2·H_3** that can furtherly recognize and open **H_4**, leading to the generation of a new HCR trigger sequence. Thus the successive cross-opening of these hairpin reactants leads to the autonomous assembly of long dsDNA nanowires that are decorated with two different tandem DNAzymes, from which one tandem-assembled DNAzyme (**D1**) is used to produce new HCR triggers for reversely promoting the initial HCR amplifier and the other concatenated DNAzyme (**D2**) is used as an efficient signal transducer. These feedback DNAzymes catalyze the cyclic cleavage of functional duplex DNAzyme substrate for generating numerous new triggers, which can then substantially initiate a new round of HCR-assembled long DNAzyme nanowires. Concomitantly, these transducer DNAzymes can efficiently cleave the ribonucleotide (**rA**)-containing substrates that are functionalized with a fluorophore/quencher pair at its 5'- and 3'-end, resulting in a turn-on fluorescence readout signal.

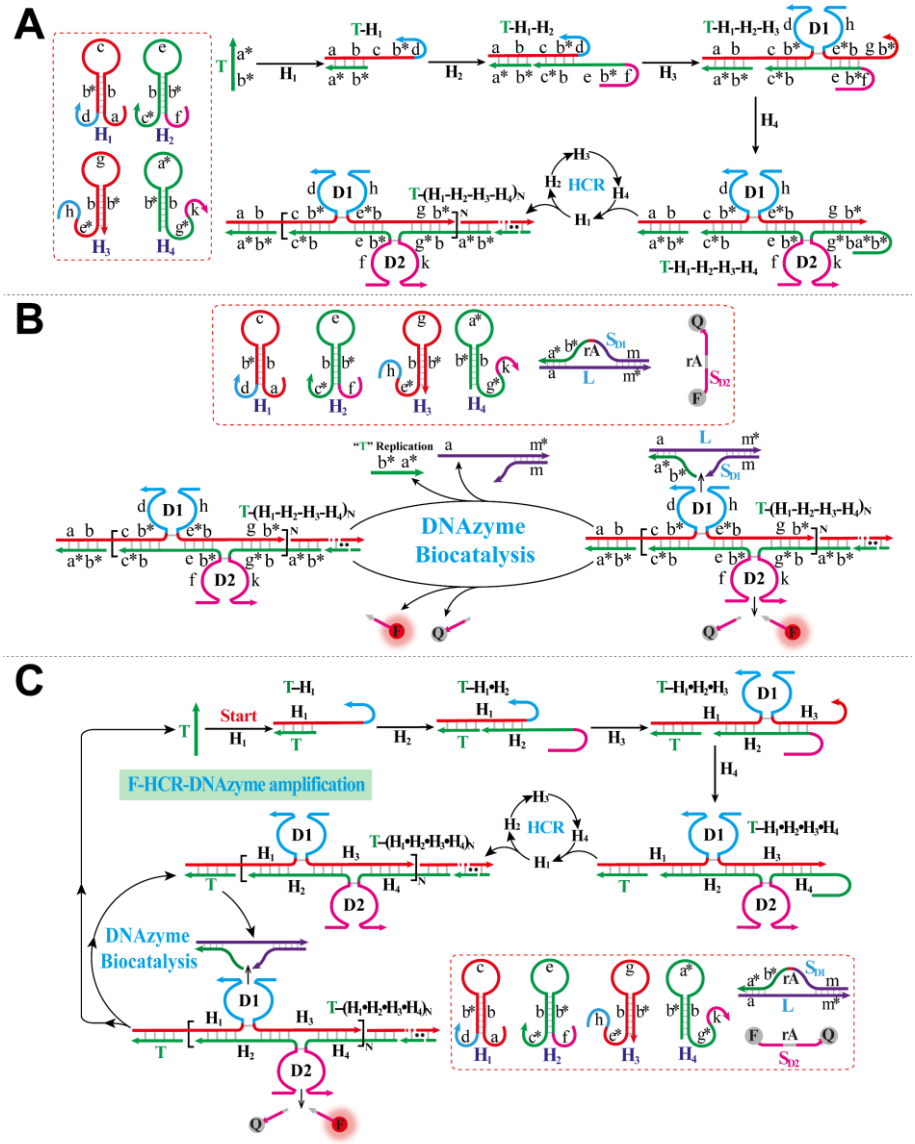

Figure S1. Schematic illustration of the HCR system (A), the HCR-assembled DNAzyme biocatalysis (B), the F-HCR-DNAzyme amplification platform (C).

Simulation of F-HCR-DNAzyme hairpin reactants

To avoid signal leakage of F-HCR-DNAzyme system, all of the hairpin reactants of F-HCR-DNAzyme system need to be carefully designed with a metastable structure by the aid of NUPACK software.[5]

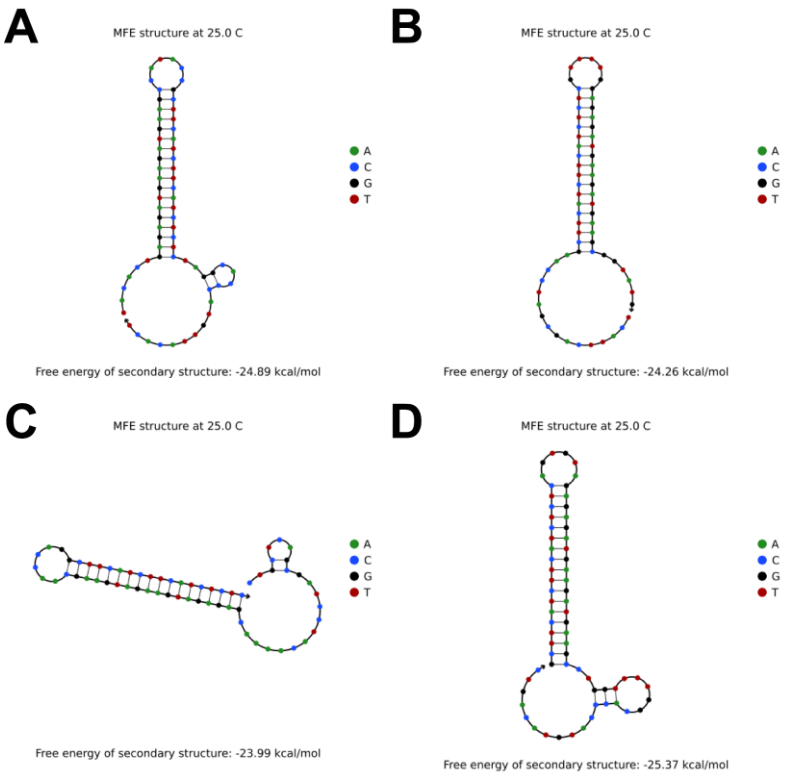

Figure S2. Theoretical simulation of the secondary hairpin structures of (A) $\mathbf{H_1}$, (B) $\mathbf{H_2}$, (C) $\mathbf{H_3}$, and (D) $\mathbf{H_4}$ probes for integrating the F-HCR-DNAzyme system.

Optimization of substrate blocker

The strand **L** is used to block the DNAzyme substrate $\mathbf{S_{D1}}$ to avoid the annoying signal leakage of the F-HCR-DNAzyme system yet to retain the efficient DNAzyme-catalyzed cleavage of $\mathbf{S_{D1}}$-**L** duplex. The interaction between **L** and the exposed **T** of $\mathbf{S_{D1}}$ should be moderate to initiate the subsequent HCR after the DNAzyme-mediated cleavage of $\mathbf{S_{D1}}$-**L** duplex. Thus, the **L** strand plays a key role in promoting the signal-to-background ratio of the F-HCR-DNAzyme system, and needs to be optimized. Here, three different blocker strands with different lengths and mutant sites ($\mathbf{L_{14}}$, $\mathbf{L_{15}}$ and $\mathbf{L_{16}}$, details see **Table S1** in supporting information) were rationally designed and investigated. According to the fluorescence response of F-HCR-DNAzyme system, the blocker $\mathbf{L_{15}}$ contributed to the highest fluorescence increasement (**Figure S3**) with a comparably lower background signal, and was selected for the F-HCR-DNAzyme system.

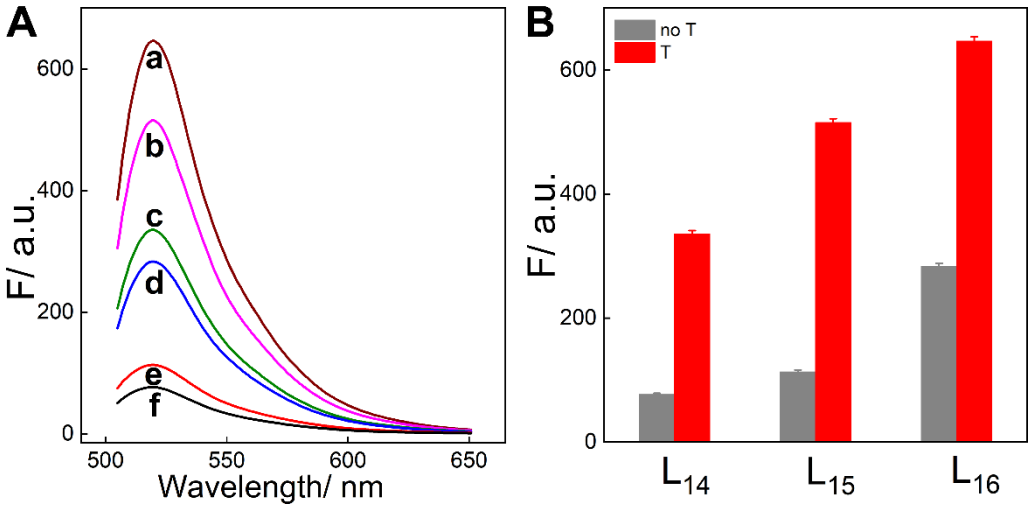

Figure S3. (A) Fluorescence spectra of the different blocker $\mathbf{L_{16}}$ (a/d), $\mathbf{L_{15}}$ (b/e), $\mathbf{L_{14}}$ (c/f)-involved F-HCR-DNAzyme systems with/without trigger **T** (50 nM). (B) Summarized fluorescence intensity changes of the different F-HCR-DNAzyme systems as shown in (A). Error bars were derived from n = 3 experiments.

Optimization of the ratio of substrate to blocker

In F-HCR-DNAzyme amplifier, the blocker strand **L** is used to hybridize with the **T** analogue domain of $\mathbf{S_{D1}}$ to avoid signal leakage. However, excess **L** might further hybridize with the cleaved trigger **T** that otherwise prohibits the HCR process. Therefore, the ratio of $\mathbf{S_{D1}}$ to **L** needs also optimized. According to the fluorescence changes of F-HCR-DNAzyme system, the system with $\mathbf{S_{D1}}$/$\mathbf{L_{15}}$ of 1:1.25 contributed to the highest fluorescence increasement with comparably lower signal leakage (**Figure S4**), thus was chosen for the following experiments.

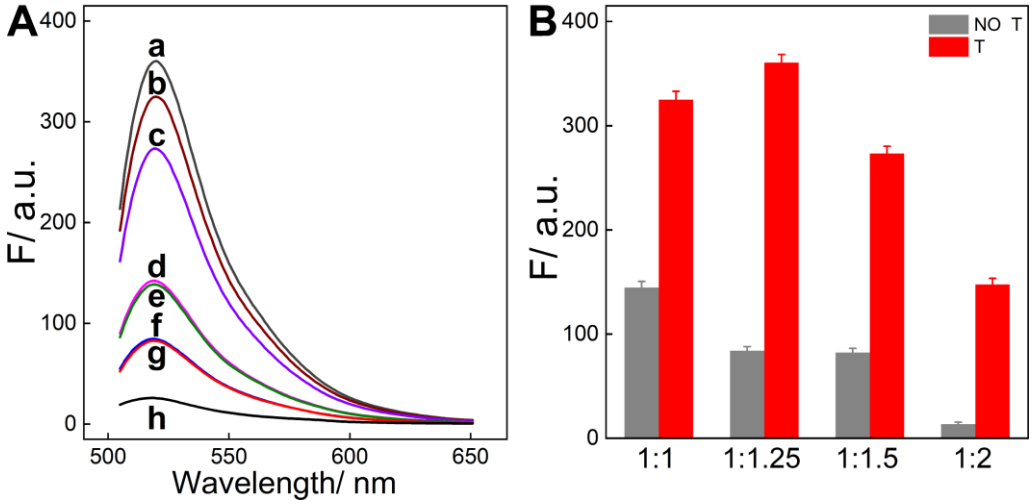

Figure S4. (A) Fluorescence response of the F-HCR-DNAzyme systems consisting of different ratios of $\mathbf{S_{D1}}$ to **L**: (a/f) 1:1.25, (b/e) 1:1, (c/g) 1:1.5 and (d/h) 1:2, in the presence/absence of **T** (25 nM). (B) Summarized fluorescence intensity changes of the different F-HCR-DNAzyme systems as shown in (A). Error bars were derived from n = 3 experiments.

Demonstration of the functions of DNAzyme circuit

The feasibility of the HCR-DNAzyme system was explored. To demonstrate the DNAzyme-mediated feedback principle of the F-HCR-DNAzyme system, the substrate **S_{D1}** was substituted with a mutant substrate **S_{D1}'** to get a Non-F-HCR-DNAzyme system. Here the chimeric **rA** of substrate **S_{D1}** was substituted with deoxyribonucleotide **A** to obtain **S_{D1}'** that could not be cleaved by DNAzyme **D1**, while substrate **S_{D2}** was unaffected to achieve **D2**-involved efficient signal transduction. As compared with the Non-F-HCR-DNAzyme system, the F-HCR-DNAzyme system revealed a much higher fluorescence readout (**Figure S5**) in the presence of trigger **T** and was encoded with almost identical background signal without **T**. This indicated that all reactants were metastable and can be only initiated by **T** of interest. In addition, the reverse **D1**-generated new HCR triggers **T** could indeed motivate the initial HCR circuit, and thus contribute to the synergistically amplified cross-activation of HCR and DNAzyme constitutes.

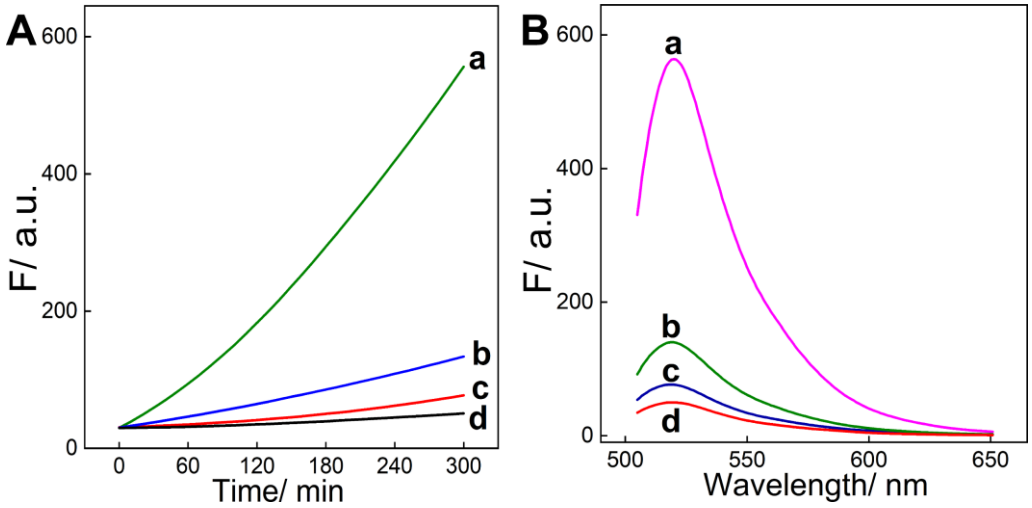

Figure S5. (A) Time-dependent fluorescence changes (at λ_{em}=520 nm) and (B) the corresponding fluorescence spectra (at 5 h) of F-HCR-DNAzyme (a/c) and Non-F-HCR-DNAzyme (b/d) systems with/without trigger **T** (50 nM).

Demonstration of the indispensable role of HCR circuit

The specific function of HCR system was verified by expelling one of the hairpin reactants (**H**$_1$, **H**$_2$, **H**$_3$, or **H**$_4$) from the F-HCR-DNAzyme system. The respective fluorescence spectra of these different systems were acquired and displayed in **Figure S6A**. **Figure S6B** shows the corresponding summarized fluorescence variations. Clearly, almost no fluorescence change was observed for the respective **T**-triggered systems when the hairpin reactant **H**$_1$, **H**$_2$, **H**$_3$ or **H**$_4$ was removed from the F-HCR-DNAzyme system. Thus all of these HCR hairpin reactants are indispensable for carrying out the F-HCR-DNAzyme system with all of these involved hairpins. This demonstrated that the cross-activated HCR-DNAzyme system started with the HCR circuit and got through successive cross-activated feedback reaction accelerations.

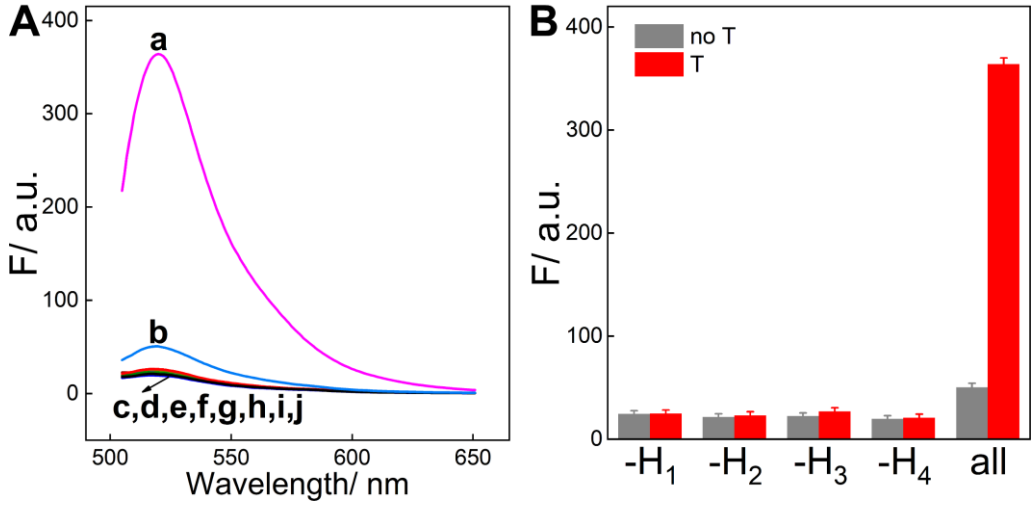

Figure S6. (A) Fluorescence spectra of the F-HCR-DNAzyme system in the presence of (a) **H**$_1$+**H**$_2$+**H**$_3$+**H**$_4$+**T**, (b) **H**$_1$+**H**$_2$+**H**$_3$+**H**$_4$, (c) **H**$_2$+**H**$_3$+**H**$_4$+**T**, (d) **H**$_2$+**H**$_3$+**H**$_4$, (e) **H**$_1$+**H**$_3$+**H**$_4$+**T**, (f) **H**$_1$+**H**$_3$+**H**$_4$, (g) **H**$_1$+**H**$_2$+**H**$_4$+**T**, (h) **H**$_1$+**H**$_2$+**H**$_4$, (i) **H**$_1$+**H**$_2$+**H**$_3$+**T** and (j) **H**$_1$+**H**$_2$+**H**$_3$. (B) Summarized fluorescence intensity changes of the different F-HCR-DNAzyme systems as shown in (A). The concentration of **T** is 25 nM and error bars are derived from n = 3 experiments.

AFM characterization of F-HCR-DNAzyme product

As shown in **Figure S7**, the target-triggered F-HCR-DNAzyme generates a large amount of micrometer-long linear products with a height of ~1.5 nm (**Figure S7** inset), which corresponds to the height of dsDNA. This confirms that the F-HCR-DNAzyme system proceeded *via* promoting the efficient HCR-assembled dsDNA nanowires as expected.

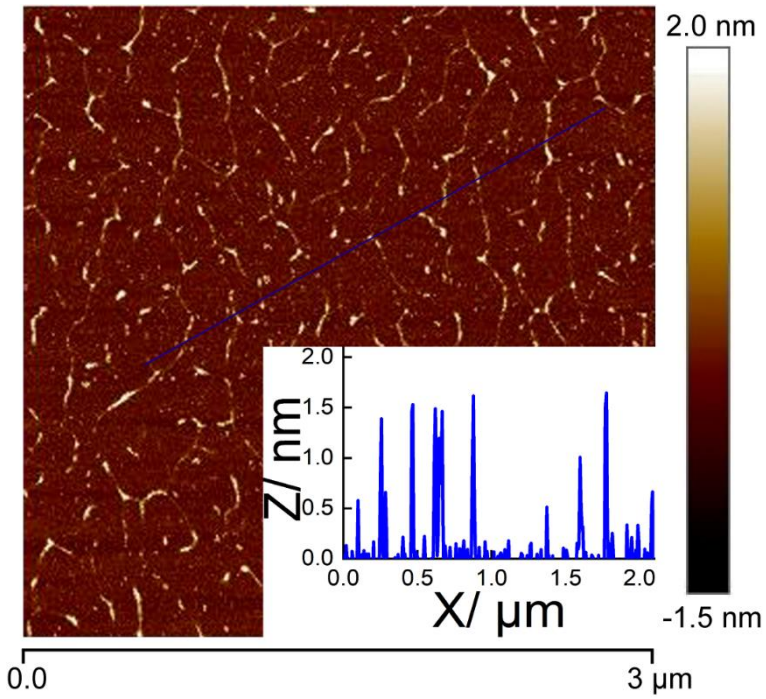

Figure S7. AFM characterization of the F-HCR-DNAzyme-assembled DNA product in the presence of trigger **T**. Detailed preparation condition is referred to the experimental section.

Non-F-HCR-DNAzyme-mediated biosensing

To assess the sensing performance of the Non-F-HCR-DNAzyme system, the substrate of feedback DNAzyme (**S**$_{D1}$) was replaced with a non-cleaved substrate (**S**$_{D1}$') to get a Non-F-HCR-DNAzyme system. As shown in **Figure S8**, 5 nM trigger **T** generates identical fluorescence increscent as compared with background, indicating a limited sensitivity of the Non-F-HCR-DNAzyme system.

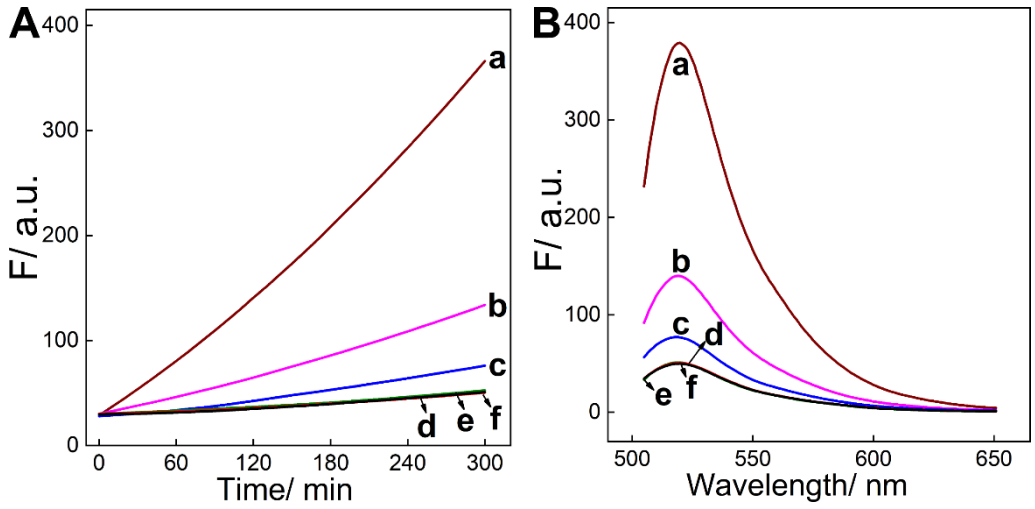

Figure S8. (A) Time-dependent fluorescence changes (at λ_{em}=520 nm) generated by the Non-F-HCR-DNAzyme system upon analyzing varied concentrations of **T**: (a) 1×10^{-7} M, (b) 5×10^{-8} M, (c) 2×10^{-8} M, (d) 5×10^{-9} M, (e) 1×10^{-9} M and (f) 0 M. (B) The corresponding fluorescence spectra of the Non-F-HCR-DNAzyme system after 5 h.

Optimization of miR-21-targeting auxiliary module

The updated miR-21-targeting F-HCR-DNAzyme platform is composed of the recognition hairpin and the feedback HCR-DNAzyme amplicon. MiR-21 recognizes and opens the recognition hairpin to release trigger **T** for the following cross-activated F-HCR-DNAzyme reaction. Thus, the recognition hairpin needs optimized to get an improved sensing performance. Ultimately, the intermediately stable **H$_5$** showed the highest fluorescence increasement with lower fluorescence background (**Figure S9**), thus was chosen as the auxiliary recognition module for the following experiments.

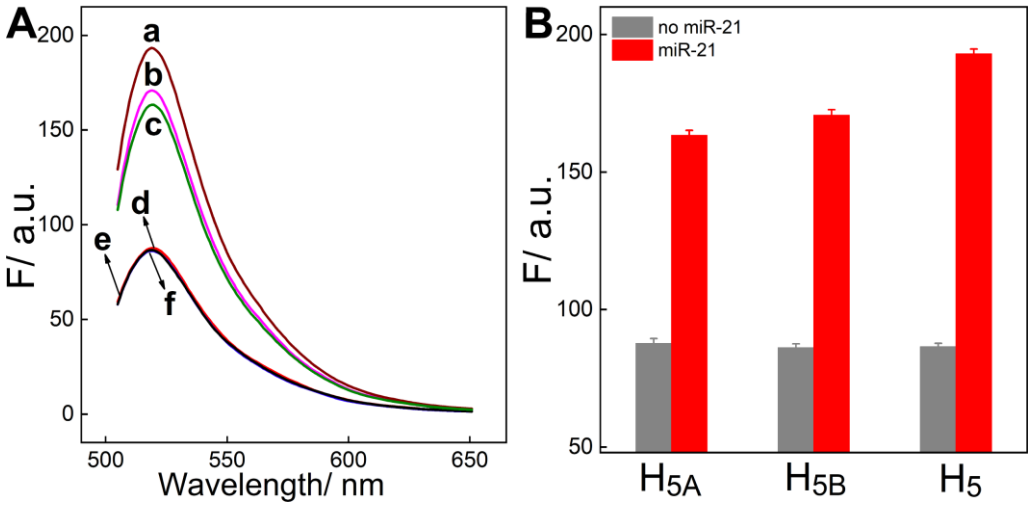

Figure S9. (A) Fluorescence spectra of **H$_5$** (a/e), **H$_{5B}$** (b/f), or **H$_{5A}$** (c/d)-integrated F-HCR-DNAzyme system with/without miR-21 (25 nM). (B) Summarized fluorescence intensity changes of the different F-HCR-DNAzyme systems as shown in (A). Error bars were derived from n = 3 experiments.

Performance of the miR-21-sensing F-HCR-DNAzyme platform

The fluorescence signal exhibits an exponential elevation with increasing concentrations of miR-21 (**Figure S10**), originating from the gradual formation of linear dsDNA nanostructure with co-localized DNAzymes for amplified HCR acceleration and signal transduction.

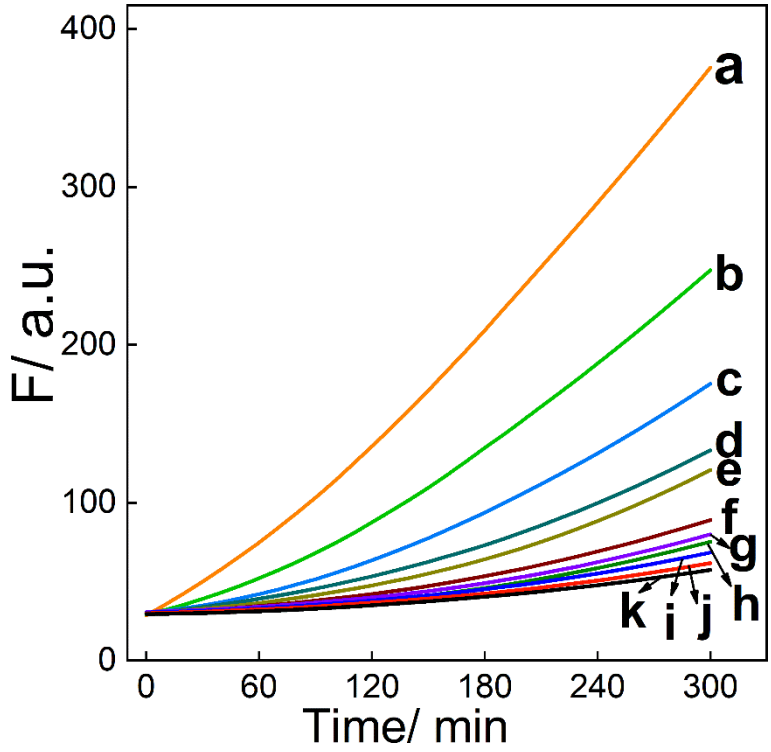

Figure S10. Time-dependent fluorescence changes of the updated miR-21-targeting F-HCR-DNAzyme system (at λ_{em}=520 nm) upon analyzing different concentrations of miR-21: (a) 1×10^{-7} M, (b) 5×10^{-8} M, (c) 2.5×10^{-8} M, (d) 1×10^{-8} M, (e) 5×10^{-9} M, (f) 1×10^{-9} M, (g) 5×10^{-10} M, (h) 1×10^{-10} M, (i) 5×10^{-11} M, (j) 1×10^{-11} M and (k) 0 M.

Colorimetric miR-21 assay *in vitro*

The F-HCR-DNAzyme system could be extensively developed as an alternative label-free sensing platform by readily adapting a different DNAzyme catalyst. This was exemplified by using hemin/G-quadruplex HRP-mimicking DNAzyme that allows the facile colorimetric transduction of analyte. Here, the Mg^{2+}-dependent RNA-hydrolyzing DNAzyme subunits of **H2** was replaced with HRP-mimicking DNAzyme, and the auxiliary hairpin **H5** was similarly introduced for recognizing miR-21. Thus, miR-21 triggered the cross-hybridization of HCR reactants for generating linear DNA nanowires with tandemly assembled feedback DNAzyme (**D1**) and transducer G-quadruplex (**D3**) nanostructures (**Figure S11A**). In the presence of hemin, these G-quadruplex DNAzyme enabled the catalytic oxidation of $ABTS^{2-}$ to colored $ABTS^{-\bullet}$ by H_2O_2. A substantial absorbance increasement of $ABTS^{-\bullet}$ was obtained with increasing concentrations of miR-21 from 50 pM to 10 nM (**Figure S11B**), demonstrating the versatile and universal transduction means of the present F-HCR-DNAzyme-amplified biosensing system.

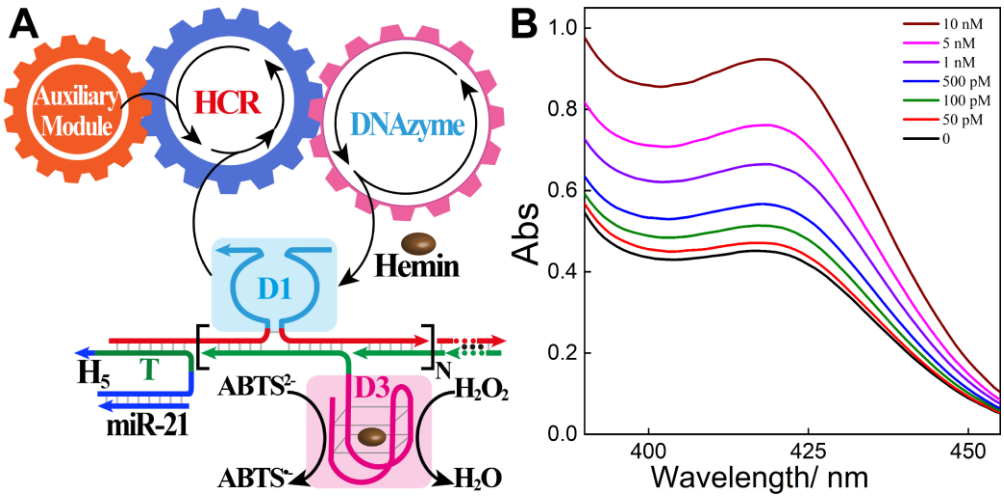

Figure S11. (A) Scheme of the extended label-free F-HCR-DNAzyme system for amplified miR-21 assay. (B) Absorbance spectra of the F-HCR-DNAzyme system upon its incubation with different concentrations of miR-21.

Incubation optimization for intracellular miR-21 imaging

As a prerequisite intracellular imaging execution, the incubation time of F-HCR-DNAzyme system was investigated by using flow cytometry. As shown in **Figure S12**, a weak fluorescence signal is acquired at 1 h of time-interval due to an inadequate uptake of the F-HCR-DNAzyme reactants with insufficient reaction duration. While the fluorescence intensifies with increasing incubation time, and reaches a saturation value at 4 h, which is thus chosen as the optimized incubation time for the following intracellular imaging experiments.

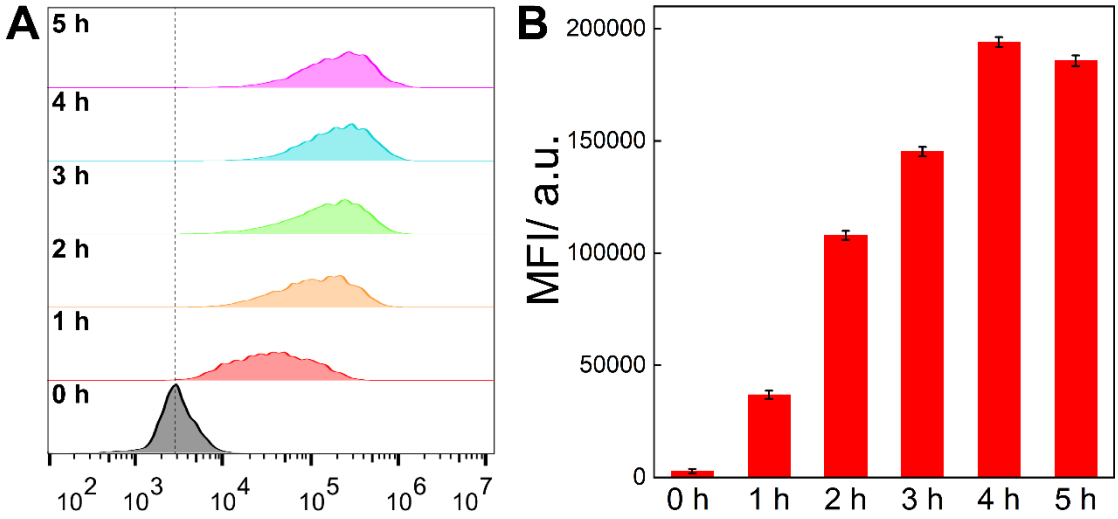

Figure S12. (A) Flow cytometry assay of MCF-7 cells incubated with the F-HCR-DNAzyme system for different time-intervals. (B) The acquired mean fluorescence intensities of these different systems as shown in (A). Error bars were derived from n = 3 experiments.

Specificity of the F-HCR-DNAzyme-mediated miR-21 imaging

MCF-7 cells were pretreated with anti-miR-21 to downregulate the intracellular miR-21 level. As expected, the anti-miR-21-pretreated MCF-7 cells revealed a lower fluorescence signal as compared with that of untreated cells (**Figure S13**), demonstrating the satisfied specificity of the miR-21-targeting F-HCR-DNAzyme nanoplatform.

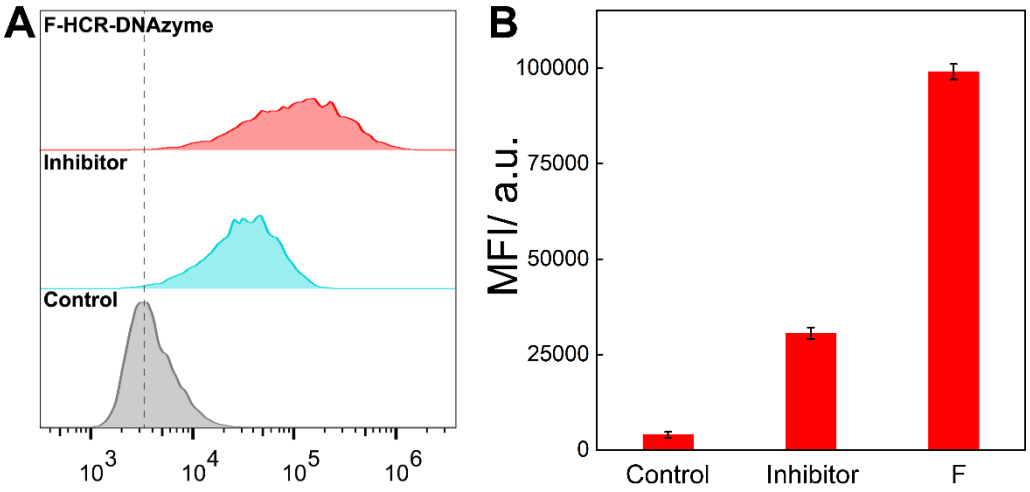

Figure S13. (A) Flow cytometry analysis and (B) the corresponding mean fluorescence intensities of differently treated MCF-7 cells by sing F-HCR-DNAzyme amplification system. Error bars were derived from n = 3 experiments.

Control experiments of intracellular imaging

To demonstrate the feasibility and amplification efficiency of the F-HCR-DNAzyme system for intracellular miR-21 imaging, more control experiments were implemented. As shown in **Figure S14**, the cells transfected with **H1**- and **H3**-subtracted F-HCR-DNAzyme amplifier revealed nearly no fluorescence readout, demonstrating that it is endogenous miR-21 that specifically triggered the F-HCR-DNAzyme amplifier to produce DNAzyme-decorated nanowires with substantially higher fluorescence output. In addition, the intact F-HCR-DNAzyme-treated MCF-7 cells revealed a much higher fluorescence readout than the Non-F-HCR-DNAzyme counterpart, which is attributed to synergistic amplification of HCR and DNAzyme amplicons.

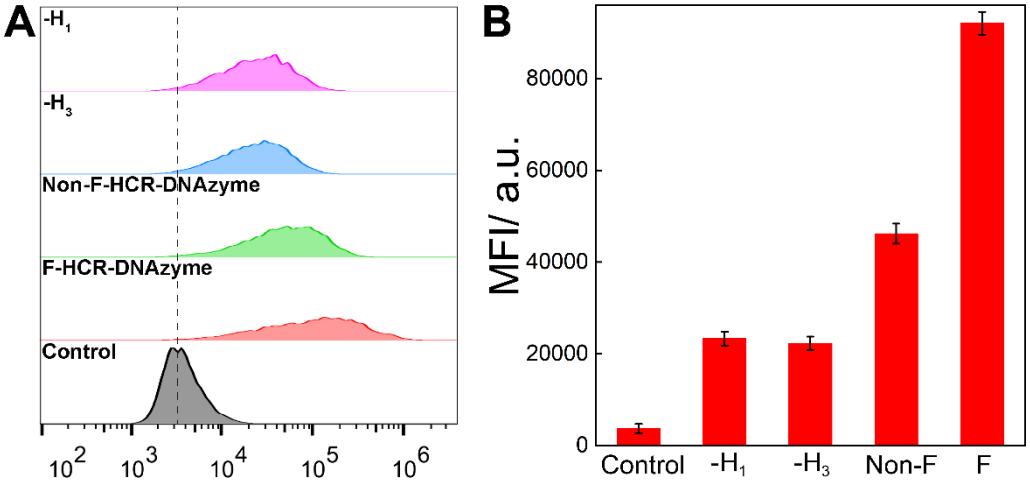

Figure S14. (A) Flow cytometry analysis of MCF-7 cells that were respectively treated with **H1**- or **H3**-excluded F-HCR-DNAzyme system, F-HCR-DNAzyme system and Non-F-HCR-DNAzyme system. (B) The corresponding mean fluorescence intensities of MCF-7 cells with different treatments. Error bars were derived from n = 3 experiments.

F-HCR-DNAzyme-based intracellular miR-21 imaging

To evaluate the performance of F-HCR-DNAzyme in different living cells, HeLa and MRC-5 cells were also chosen as important controls. According to the corresponding flow cytometric analysis (**Figure S15**), MCF-7 cells showed the highest fluorescence gain, while MRC-5 cells revealed the weakest fluorescence increasement, which were consistent with that of confocal microscopy results. These results showed that the F-HCR-DNAzyme system could distinguish different cell lines according to their different endogenous miRNA expression levels. The relative efficiency of different cells was obtained from the ratio R ($R=F/F_0$, where F represented the fluorescence intensity of cells treated with F-HCR-DNAzyme system and F_0 represented the fluorescence intensity of cells without treatment). Then, the R of MCF-7 cells was served as a standard value of 100%. Then the R values of HeLa and MRC-5 cells were respectively divided by the R of MCF-7 cells to obtain their relative efficiency.

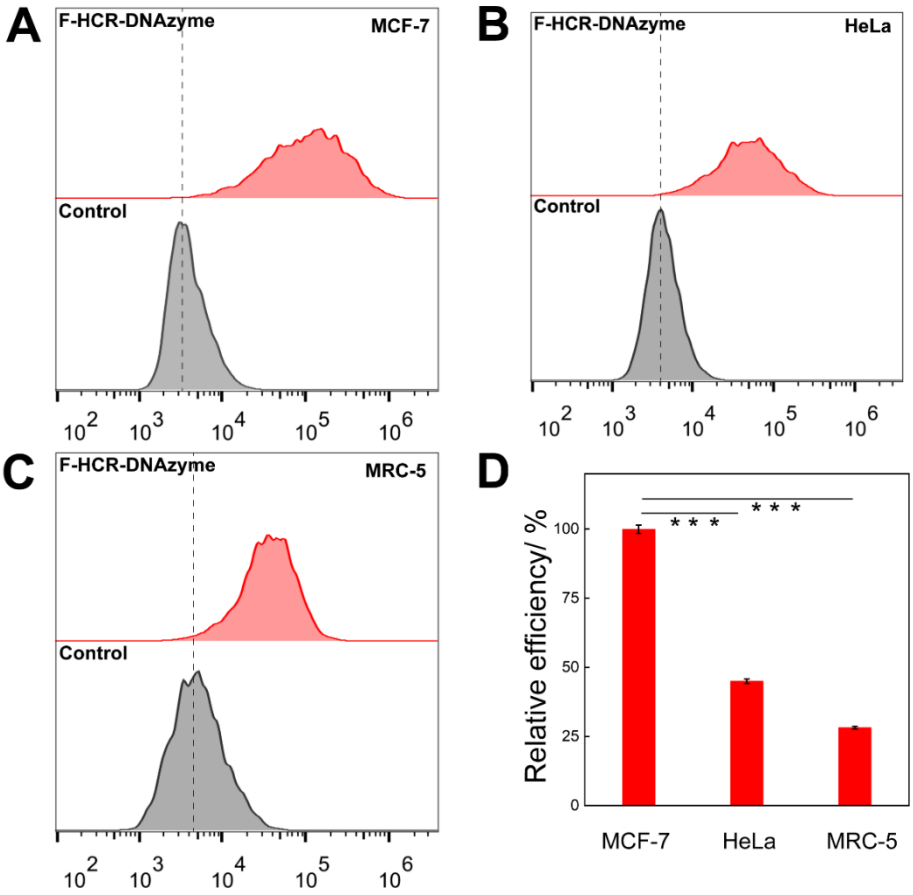

Figure S15. Flow cytometry analysis of (A) MCF-7 cells, (B) HeLa cells, (C) MRC-5 cells treated with F-HCR-DNAzyme system. (D) The relative efficiency of fluorescence gain for these different systems as shown in (A), (B) and (C). Error bars were derived from n = 3 experiments and (***) represented $p<0.001$.

References

1 F. Wang, J. Elbaz, R. Orbach, N. Magen and I. Willner, *J. Am. Chem. Soc.*, 2011, **133**, 17149-17151.

2 J. Huang, H. Wang, X. Yang, K. Quan, Y. Yang, L. Ying, N. Xie, M. Ou and K. Wang, *Chem. Sci.*, 2016, **7**, 3829-3835.

3 L. Zou, Q. Wu, Y. Zhou, X. Gong, X. Liu and F. Wang, *Chem. Commun.*, 2019, **55**, 6519-6522.

4 J. Liu, M. Cui, H. Zhou and W. Yang, *ACS Sens.*, 2017, **2**, 1847-1853.

5 J. N. Zadeh, C. D. Steenberg, J. S. Bois, B. R. Wolfe, M. B. Pierce, A. R. Khan, R. M. Dirks and N. A. Pierce, *J. Comput. Chem.*, 2011, **32**: 170-173.